Evidence for three-dimensional Dirac conical bands in TlBiSSe by optical and magneto-optical spectroscopy

F. Le Mardelé, J. Wyzula, I. Mohelsky, S. Nasrallah, M. Loh, S. Ben David, O. Toledano, D. Tolj, M. Novak, G. Eguchi, et al.

Letter | Editors' Suggestion | Featured in Physics

Evidence for three-dimensional Dirac conical bands in TlBiSSe by optical and magneto-optical spectroscopy

F. Le Mardelé,[1,2] J. Wyzula,[1,2] I. Mohelsky,[1] S. Nasrallah,[2,3] M. Loh,[2,4] S. Ben David,[2] O. Toledano,[2,5] D. Tolj,[6] M. Novak,[7] G. Eguchi,[3] S. Paschen,[3] N. Barišić,[3,7] J. Chen,[8] A. Kimura,[8,9] M. Orlita,[1,10] Z. Rukelj,[7,*] Ana Akrap,[2,†] and D. Santos-Cottin[2,‡]

[1]*LNCMI-EMFL, CNRS UPR3228, Université Grenoble Alpes, Université Toulouse, Université Toulouse 3, INSA-T, Grenoble and Toulouse, Cedex 9 38042, France*

[2]*Department of Physics, University of Fribourg, CH-1700 Fribourg, Switzerland*

[3]*Institute of Solid State Physics, TU Wien, A-1040 Vienna, Austria*

[4]*Physics Department, Stanford University, Stanford, California 94305, USA*

[5]*Departamento Física Interdisciplinar, Facultad de Ciencias, Universidad Nacional de Educación a Distancia (UNED), Avenida Esparta, E-28232 Las Rozas, Spain*

[6]*Laboratory for Quantum Magnetism, Institute of Physics, École Polytechnique Fédérale de Lausanne (EPFL), CH-1015 Lausanne, Switzerland*

[7]*Department of Physics, Faculty of Science, University of Zagreb, Bijenička 32, HR-10000 Zagreb, Croatia*

[8]*Graduate School of Advanced Science and Engineering, Hiroshima University, 1-3-1 Kagamiyama, Higashi-Hiroshima 739-8526, Japan*

[9]*International Institute for Sustainability with Knotted Chiral Meta Matter (SKCM2), 1-3-2 Kagamiyama, Higashi-Hiroshima 739-8511, Japan*

[10]*Faculty of Mathematics and Physics, Charles University, Ke Karlovu 5, CZ-121 16 Prague, Czech Republic*

(Received 14 January 2023; accepted 11 April 2023; published 1 June 2023)

TlBiSSe is a rare realization of a three-dimensional semimetal with a conically dispersing band that has an optical response which is well isolated from other contributions in a broad range of photon energies. We report optical and magneto-optical spectroscopy on this material. When the compound is chemically tuned into a state of the lowest carrier concentration, we find a nearly linear frequency dependence of the optical conductivity below 0.5 eV. Landau level spectroscopy allows us to describe the system with a massive Dirac model, giving a gap $2\Delta = 32$ meV and an in-plane velocity parameter $v_{xy} = 4.0 \times 10^5$ m/s.

DOI: 10.1103/PhysRevB.107.L241101

Research on topological semimetals is an important part of modern condensed matter physics, in great part due to relativisticlike physics which may be observed in such systems [1–3]. An important class of topological semimetals are three-dimensional (3D) Dirac semimetals [4,5]. In them, ideally a single conical band dominates the energy landscape around the Fermi level. There are not many such systems that we can easily access experimentally [6]. One such way a conical band can arise is when the bulk energy gap of a topological insulator is gradually closed [7–9], for example, by chemical tuning or high pressure [10–12]. In such a scenario, the zero-gap state is not topologically protected and a gap may easily open. In this Letter we show that TlBiSSe may be chemically tuned into a clean example of a system whose linear band dispersion dictates the electrodynamic response in a broad energy range.

We investigated the low-energy excitations by infrared spectroscopy and magnetospectroscopy of TlBiSSe single crystals with an optimized composition. The single-crystal quality of TlBiSSe was improved by using a different nominal content of Bi and Tl during synthesis. A strong decrease of the metallicity—a reduced Drude contribution—points to a shift of the Fermi level as the ratio Tl:Bi is tuned. For a specific composition (referred to as sample S_3), the system becomes a semimetal or a narrow-gap semiconductor, with the Fermi level close to the Dirac node. The real part of the optical conductivity increases linearly in photon energy up to 0.4 eV, characteristic of a 3D conical band. For the same composition, Landau level (LL) spectra confirm massive Dirac behavior with a band gap as low as $2\Delta = 32$ meV and a velocity parameter $v_{xy} = 4 \times 10^5$ m/s. Our results show that the properties of TlBiSSe depend on the synthesis quality and the ratio of Tl:Bi in the structure, which strongly shifts the Fermi level to expose the large conical band.

We synthesized single crystals of TlBiSSe with a melt-growth technique using high-purity elements, 4N or better, of Tl, Bi, S, and Se, sealed under vacuum in a quartz tube. The hexagonal crystal structure of TlBiSSe is shown in Fig. 1(a). Recent publications show that stoichiometric melt always gives electron-doped single crystals [13–15] due to bismuth substitution on the thallium site. To prevent this, it is possible to play with the initial Tl:Bi ratio to drastically reduce the carrier densities [14,16]. In this study, we prepared TlBiSSe

*rukelj@phy.hr
†ana.akrap@unifr.ch
‡david.santos@unifr.ch

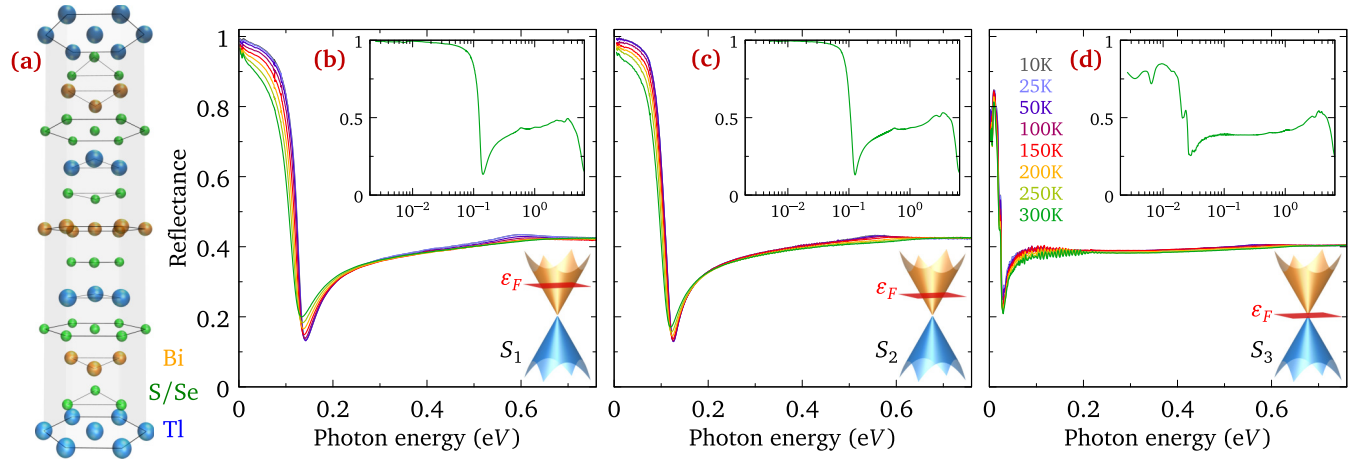

FIG. 1. (a) Hexagonal crystal structure of TlBiSSe. (b)–(d) Reflectance for the samples S_1, S_2, and S_3 up to 0.8 eV for various temperatures. Insets show the reflectance at 300 K in the full energy range up to 6.5 eV.

samples using three different initial ratios of Tl:Bi, starting from Tl : Bi = 1 : 1 for the synthesis of sample S_1, to Tl : Bi = 1.2 : 0.8 for sample S_2, and finally Tl : Bi = 1.5 : 0.5 for sample S_3. We confirmed the high-quality crystal structure of these samples by x-ray diffraction analysis. We showed by energy dispersive x-ray diffraction that the final compositions of our grown crystals are close to stoichiometry [17].

We measured the near-normal incidence reflectance of freshly cleaved TlBiSSe samples using a Bruker Vertex 70v spectrometer from 10 to 300 K. The sample was mounted on a cold finger and we employed the overfilling technique [18] to determine its absolute reflectance with an accuracy better than 0.5%. The data were extended to 6.5 eV at room temperature using ellipsometry measurements. To obtain the complex optical conductivity from a Kramers-Kronig analysis, we extrapolated the low-frequency reflectance with a Hagen-Rubens response. At high frequencies, we extended the measurements using the Tanner method [19], which calculates the reflectivity from the atomic x-ray scattering cross sections from 10 to 60 eV, followed by a $1/\omega^4$ free-electron behavior. We filled the gap between our experiment and the x-ray data with a smooth cubic spline curve. The infrared magnetospectroscopy measurements were performed in a superconducting coil, at 2 K and up to 16 T, while keeping the sample at 4.2 K in the He exchange gas. We measured transmission and reflection configurations in the Faraday geometry, where the static magnetic field is parallel to the propagation vector of the incident light wave. The sample measured in transmission was cleaved to a thickness of ∼10 μm. The electronic structure was calculated with the QUANTUM ESPRESSO package [20], employing projector augmented-wave pseudopotentials to simulate the core interactions [21]. We performed calculations in a $2 \times 2 \times 2$ trigonal supercell to recover the Kramers degeneracy and obtain a spin-degenerate 3D Dirac cone around the Γ point. Then, we unfolded the band structure of this supercell to a primitive trigonal cell using the BANDUP code, with more details given in the Supplemental Material [17,22–27].

Figure 1 presents the temperature-dependent reflectance, as a function of the photon energy, measured for three different batches of TlBiSSe single crystals: S_1, S_2, and S_3. The insets show the full energy range measurements performed at room temperature. In the low-energy range, the reflectance of samples S_1 and S_2, in Figs. 1(b) and 1(c), respectively, shows a similar response, typical of a system with a small Fermi surface. The 10 K reflectance tends to unity at very low energy, $R(\omega \to 0) \to 1$. The reflectance in that range strongly decreases with the increase of the temperature. Around 100 meV, the reflectance of both samples dramatically drops by about 80% at the screened plasma edge. The sharp plasma edges indicate that the Drude scattering rate in both samples is fairly low.

In contrast, the low-energy reflectance of sample S_3 in Fig. 1(d) shows a response more characteristic of an undoped semiconductor or a semimetal, with several strong phonon modes below 30 meV. The intensity of these modes decreases with the increase of temperature. The reflectance for the composition S_3 does not approach unity at the lowest attained energies, although it has a weak upturn. The strong edge seen at 20 meV is not related to Drude carriers, but is rather linked to a strong phonon response. Moreover, in sample S_3 we observe clear oscillations in the reflectance between 50 and 200 meV. These are Fabry-Pérot interference fringes caused by a transparent energy window in this sample.

Overall, the plasma edge shifts a little towards lower energies moving from sample S_1 to sample S_2, while for sample S_3 the free-carrier plasma edge moves outside of our experimental window. This means that the carrier density strongly decreases as we tune the composition from S_1 to S_3 by increasing the Tl:Bi ratio. This initial observation is in line with the previous transport measurements [14,16]. At higher energies, all three samples present a similar reflectance behavior: (1) an almost flat region in the range 250–800 meV with a reflectance value of around 0.4, (2) a small bump at 10 K around 550–600 meV, weakened at higher temperatures, and (3) a strong decrease of the intensity above 2.5 eV at 300 K.

Figures 2(a)–2(c) show the energy dependence of the real (dissipative) part of the optical conductivity $\sigma_1(\omega)$ in the low-energy range. Each panel corresponds to a different composition, from S_1 to S_3. At low energies, $\sigma_1(\omega)$ of samples S_1 and S_2 shows a well-defined Drude peak, which narrows with a decreasing temperature. For the 10 K data, we fit

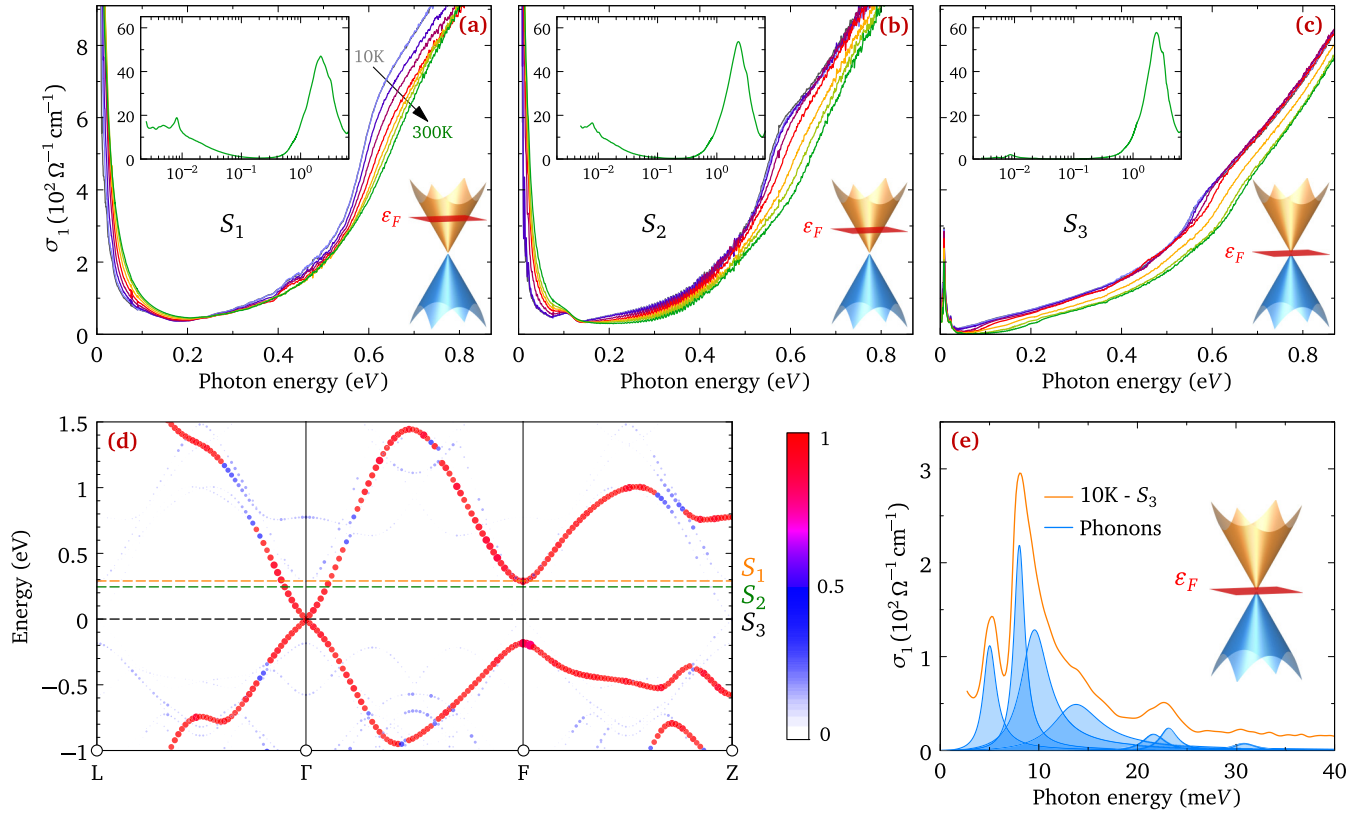

FIG. 2. Energy dependence of the real part of the optical conductivity $\sigma_1(\omega)$ for samples (a) S_1, (b) S_2, and (c) S_3. The main panels show the low-energy range, while the insets show the full energy range of $\sigma_1(\omega)$ at 300 K on a logarithmic scale. The optical conductivity is obtained from Kramers-Kronig transformation on the reflectance data shown in Fig. 1. (d) Band-structure calculations in a trigonal primitive cell after unfolding the $2 \times 2 \times 2$ trigonal supercell band structure. The blue color scale represents the amplitude of the supercell eigenstates projection into the primitive cell eigenstates [17]. Dashed lines indicate the approximate positions of the Fermi level for the three samples. (e) Low-energy optical conductivity including a fit of the phonon modes [28].

the reflectance of samples S_1 and S_2 [17,28] and obtain unscreened plasma frequencies of around 540 and 490 meV, with scattering rates of ∼3.2 and ∼2.5 meV, respectively. For both samples, $\sigma_1(\omega)$ has a poorly conducting intermediate-energy region immediately above the Drude component, ending with a sudden onset of absorption around 550 meV. Comparing with the band-structure calculation in Fig. 2(d), we may assign this absorption onset to transitions near the F point in the Brillouin zone [29]. Overlaying the curves of the samples S_1 and S_2, we notice a relative shift of around 40 meV of the absorption onset which allows us to estimate the position of their Fermi levels. We may place them at $\varepsilon_F \sim 280$ meV above the Dirac node for sample S_1, and at $\varepsilon_F \leqslant 260$ meV for sample S_2. A rough sketch of the Fermi-level position is given in Fig. 2(d), plotted on top of the density functional theory (DFT)-calculated bands.

On the other hand, $\sigma_1(\omega)$ of sample S_3 does not contain any visible Drude contribution, most likely because it is very narrow and limited to energies which are too low for us to access optically. Instead, several infrared active phonon modes can be seen at approximately 5, 8, 14, and 23 meV, with a possible weak mode at ∼30 meV. All these modes are shown in Fig. 2(e). We notice that the phonon modes are generally rather broad, which may be caused by disorder in the chemical structure. An obvious source of such disorder comes from a random distribution of S and Se atoms, which occupy the same lattice positions. The dc anisotropy resistivity measurements performed on sample S_3 [17,30–32] show poorly metallic behavior both in the *ab* plane and along the *c* axis. However, we obtain a very low dc conductivity value of around 310 $\Omega^{-1}\,\mathrm{cm}^{-1}$ in the *ab* plane, one order of magnitude smaller when compared to the value of similar crystals obtained in a previous study [14].

The absence of a Drude term in the optical conductivity confirms that increasing the initial Tl:Bi ratio can drastically reduce the carrier density in this system and shift the Fermi level closer to the Dirac node [14,16]. When the Fermi level is in close vicinity to the Dirac node, the low-energy interband transitions become apparent through a linear energy dependence of $\sigma_1(\omega)$ in the range 35–320 meV. At higher energies, an additional contribution kicks in at around 520 meV, and as in samples S_1 and S_2, it may be assigned to transitions near the F point of the Brillouin zone.

Finally, the optical conductivity at 300 K in the very high-energy region of all three samples is shown in the insets of Figs. 2(a)–2(c). A strong interband transition appears around 2.5 eV. This peak in $\sigma_1(\omega)$ is a fingerprint of a van Hove singularity or a saddle point. It appears because of the Dirac band folding, which can be seen as a plateau in the Γ-F direction in Fig. 2(d). Such a saddle point often leads to strong interband transitions and may be seen in the optical conductivity of several Dirac systems [33–38].

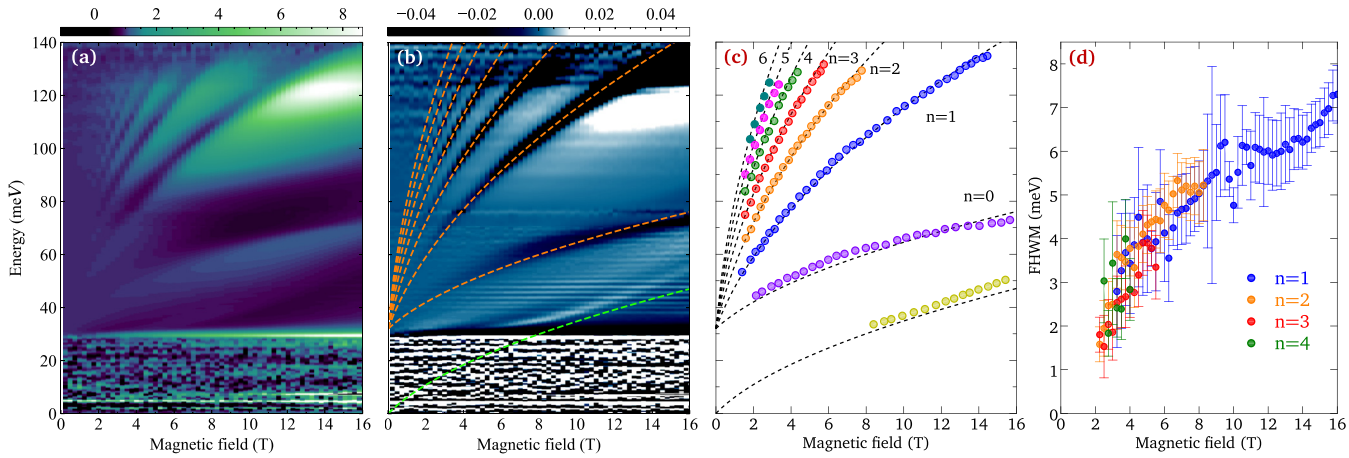

FIG. 3. Color plot of (a) the relative magnetotransmission measured at 4.2 K, T_B/T_0, and (b) its derivative d/dB (T_B/T_0). (c), (d) Magnetic field dependence of the energy positions and FWHM of the LLs fitted using Gaussian distributions.

The band dispersion is visible in zero-field optical conductivity through the density of states (DOS). However, for a system with a very small carrier density, it can be instructive to apply an external magnetic field. Since the sample S_3 has a low reflectance, in the magnetoreflection measurements we only observe two broad intra-LL excitations crossing the phonon modes in the low energy up to 45 meV [17]. Figure 3(a) shows the relative magnetotransmission T_B/T_0, where the transmission of sample S_3 in a magnetic field B is divided by its transmission at zero magnetic field. The transmission is measured in the energy range 30–140 meV. This is the exact region where we observe the Fabry-Pérot interference fringes in the zero-field reflectivity measurement discussed above [see Fig. 1(d)]. The transmission energy derivative is shown in Fig. 3(b). A series of inter-LL transitions can be seen in both magnetotransmission and its derivative. Those transitions extrapolate to a finite energy in the limit of a vanishing magnetic field, which implies a finite band gap. Moreover, the transitions are sublinear in magnetic field. This is a signature of a strongly nonparabolic band dispersion. We can fit the energies of inter-LL transitions using a massive Dirac model, shown in Fig. 3(b) [17]. In this model, assuming $k = 0$, each LL has an energy given by

$$\varepsilon_n^{\pm}(B) = \pm\sqrt{2\hbar e v_{xy}^2 Bn + \Delta^2}, \tag{1}$$

where n is an integer, 2Δ is the band gap, and the parameter v_{xy} is the in-plane asymptotic velocity of the Dirac cone.

Figures 3(c) and 3(d) show the energies of the observed inter-LL transitions as a function of B, together with the corresponding full width at half maximum (FWHM) of each transition, extracted using a Gaussian fit. Interestingly, the FWHM of the inter-LL excitations increases monotonically with the magnetic field. Finally, the dashed lines in Figs. 3(b) and 3(c) show the results of the inter- and intra-LL transition fits, using a selection rule $n \to n \pm 1$. The performed fitting procedures result in the following parameters: the band gap $2\Delta \sim 32$ meV and in-plane velocity $v_{xy} = 4.0 \times 10^5$ m/s. This velocity parameter is close to the slope of the conical band measured by photoemission [39,40], and also comparable to other similar systems with conical bands [6,41,42].

The slope of the conical band also enters the linear part of $\sigma_1(\omega)$ in Fig. 2(c). For a 3D conical band system, the low-energy σ_1 at zero temperature is described by [43–46]

$$\sigma_1(\omega) = g\frac{\sigma_0}{6\pi}\frac{\hbar\omega}{v}\Theta(\hbar\omega - 2\varepsilon_F), \tag{2}$$

where ε_F is defined from the middle of the gap, $\sigma_0 = e^2/(4\hbar) = 6 \times 10^5\ \Omega^{-1}$, v is the velocity parameter related to the slope of the conical bands, and g is the Dirac cone degeneracy. Here, g combines the spin and valley degeneracy and in our case $g = 2$, since we have a spin-degenerate Dirac cone at the Γ point. The above formula is also approximately valid for the massive Dirac case when the photon energy $\hbar\omega \sim \varepsilon_F \gg \Delta$, where the band gap $2\Delta = 32$ meV is obtained from the magneto-optical measurements.

However, comparing the result of Eq. (2) with the optical conductivity data in Fig. 2(c) implies the velocity 1.8×10^5 m/s, a value significantly lower than the above extracted v_{xy}. One reason for such a disagreement is that σ_1 probes the joint density of states, reflecting the dispersion of electrons in all three spatial directions, while photoemission and magneto-optics provide information on the in-plane band dispersion. Previous calculations of the electronic band structure [29,47] suggest that the out-of-plane velocity v_z is approximately half the in-plane velocity v_{xy}. Such an in-plane versus out-of-plane anisotropy is also indicated by our transport measurements which give a dc anisotropy ratio $\rho_z/\rho_{xy} \sim 2.7$, shown in Fig. S5 [17,30–32]. We can assume that the Dirac cone is nearly isotropic in the xy plane. In that case, for the sample S_3 we obtain $v_z \approx 1.8 \times 10^5$ m/s. This result is in fair agreement with the band structure.

Supposing a rigid band shift for the three different dopings S, together with the extracted velocities and Drude model parameters, we obtain approximate Fermi levels $\varepsilon_F \simeq 290$ and 240 meV for the samples S_1 and S_2 [17]. These values are in good agreement with the estimates from the onset of absorption in Fig. 2. Finally, with the value of the Fermi level and the asymptotic velocities, we estimate, assuming solely a Dirac cone, the total electron concentrations n for samples S_1 and S_2 to be $n_1 = 5.6 \times 10^{19}$ cm^{-3} and $n_2 = 2.9 \times 10^{19}$ cm^{-3} [17].

These values agree well with the previous magnetotransport measurements [14].

The lowest inter-LL transition sets in at 2–3 T [see Figs. 3(a) and 3(b)], which gives us the quantum limit of this sample composition. This is the field for which all the carriers are confined to the lowest LL. In the S_3 sample, a considerable chemical disorder is present and reflected, e.g., in the width of the observed phonon lines. In such a situation, it may be surprising that we do observe such a well-defined quantization of Landau levels. In fact, the S_3 sample has a relatively low electron density, and consequently, the Fermi energy ε_F lies relatively close to the weakly gapped Dirac point. In such a case, the corresponding cyclotron mass, defined classically as $m_c = \varepsilon_F/v^2$, is small and implies a sufficiently large spacing of LLs to overcome the impact of disorder.

In conclusion, we have shown that TlBiSSe is indeed a 3D Dirac system with an anisotropic band dispersion along the c axis. Tuning the Tl:Bi ratio during the growth can bring the Fermi level near the neutrality point. Our zero-field optical spectra show signatures of a broad range linear band dispersion, up to 0.4 eV, leading to the optical conductivity linear in energy, $\sigma_1(\omega) \propto \hbar\omega$. The magneto-optical spectra show a series of inter-LL transitions which confirm that the in-plane dispersion of the bands in the lowest-carrier-density sample is nearly linear, with a small band gap of $2\Delta \sim 32$ meV and an in-plane velocity of 4.0×10^5 m/s. Therefore, TlBiSSe represents a clean example of a 3D Dirac semimetal which hosts a a single conical band defining the optical and magneto-optical response in a broad range of photon energies.

We thank P. Hofegger for technical support. A.A. acknowledges funding from the Swiss National Science Foundation through Project No. PP00P2_202661. This research was supported by the NCCR MARVEL, a National Centre of Competence in Research, funded by the Swiss National Science Foundation (Grant No. 205602). D.S-C. acknowledges SPARK Grant No. CRSK-2_196610 from the Swiss National Science Foundation. Z.R. was funded by QautiXLie Centre of Excellence (Grant No. KK.01.1.1.01.0004). M.N. and N.B acknowledge support of CeNIKS project co-financed by the Croatian Government and the EU through the European Regional Development Fund Competitiveness and Cohesion Operational Program (Grant No. KK.01.1.1.02.0013). S.N. and N.B acknowledge the support of the European Research Council (ERC Consolidator Grant No. 725521). A.K. acknowledges financial support from funding from KAKENHI (No. 17H06138 and No. 18H03683). This work has been supported by the ANR projects DIRAC3D (ANR-17-CE30-0023) and COLECTOR (ANR-19-CE30-0032). We acknowledge the support of LNCMI-CNRS, a member of the European Magnetic Field Laboratory (EMFL).

[1] A. F. Young and P. Kim, Nat. Phys. **5**, 222 (2009).
[2] P. E. C. Ashby and J. P. Carbotte, Phys. Rev. B **89**, 245121 (2014).
[3] J. Wyzula, X. Lu, D. Santos-Cottin, D. K. Mukherjee, I. Mohelský, F. Le Mardelé, J. Novák, M. Novak, R. Sankar, Y. Krupko, B. A. Piot, W.-L. Lee, A. Akrap, M. Potemski, M. O. Goerbig, and M. Orlita, Adv. Sci. **9**, 2105720 (2022).
[4] N. P. Armitage, E. J. Mele, and A. Vishwanath, Rev. Mod. Phys. **90**, 015001 (2018).
[5] J. Xiong, S. K. Kushwaha, T. Liang, J. W. Krizan, M. Hirschberger, W. Wang, R. J. Cava, and N. P. Ong, Science **350**, 413 (2015).
[6] I. Crassee, R. Sankar, W. L. Lee, A. Akrap, and M. Orlita, Phys. Rev. Mater. **2**, 120302 (2018).
[7] B.-J. Yang and N. Nagaosa, Nat. Commun. **5**, 4898 (2014).
[8] R. J. Cava, H. Ji, M. K. Fuccillo, Q. D. Gibson, and Y. S. Hor, J. Mater. Chem. C **1**, 3176 (2013).
[9] Y. Ando, J. Phys. Soc. Jpn. **82**, 102001 (2013).
[10] T. Sato, K. Segawa, K. Kosaka, S. Souma, K. Nakayama, K. Eto, T. Minami, Y. Ando, and T. Takahashi, Nat. Phys. **7**, 840 (2011).
[11] T. Arakane, T. Sato, S. Souma, K. Kosaka, K. Nakayama, M. Komatsu, T. Takahashi, Z. Ren, K. Segawa, and Y. Ando, Nat. Commun. **3**, 636 (2012).
[12] X. Xi, C. Ma, Z. Liu, Z. Chen, W. Ku, H. Berger, C. Martin, D. B. Tanner, and G. L. Carr, Phys. Rev. Lett. **111**, 155701 (2013).
[13] K. Kuroda, M. Ye, A. Kimura, S. V. Eremeev, E. E. Krasovskii, E. V. Chulkov, Y. Ueda, K. Miyamoto, T. Okuda, K. Shimada, H. Namatame, and M. Taniguchi, Phys. Rev. Lett. **105**, 146801 (2010).
[14] M. Novak, S. Sasaki, K. Segawa, and Y. Ando, Phys. Rev. B **91**, 041203(R) (2015).
[15] K. Segawa, Sci. Technol. Adv. Mater. **16**, 014405 (2015).
[16] K. Kuroda, G. Eguchi, K. Shirai, M. Shiraishi, M. Ye, K. Miyamoto, T. Okuda, S. Ueda, M. Arita, H. Namatame, M. Taniguchi, Y. Ueda, and A. Kimura, Phys. Rev. B **91**, 205306 (2015).
[17] See Supplemental Material at http://link.aps.org/supplemental/10.1103/PhysRevB.107.L241101 for additional data to support our work.
[18] C. C. Homes, M. Reedyk, D. A. Cradles, and T. Timusk, Appl. Opt. **32**, 2976 (1993).
[19] D. B. Tanner, Phys. Rev. B **91**, 035123 (2015).
[20] P. Giannozzi, S. Baroni, N. Bonini, M. Calandra, R. Car, C. Cavazzoni, D. Ceresoli, G. L. Chiarotti, M. Cococcioni, I. Dabo, A. Dal Corso, S. de Gironcoli, S. Fabris, G. Fratesi, R. Gebauer, U. Gerstmann, C. Gougoussis, A. Kokalj, M. Lazzeri, L. Martin-Samos *et al.*, J. Phys.: Condens. Matter **21**, 395502 (2009).
[21] G. Kresse and D. Joubert, Phys. Rev. B **59**, 1758 (1999).
[22] P. V. C. Medeiros, S. Stafström, and J. Björk, Phys. Rev. B **89**, 041407(R) (2014).
[23] P. V. C. Medeiros, S. S. Tsirkin, S. Stafström, and J. Björk, Phys. Rev. B **91**, 041116(R) (2015).
[24] V. Popescu and A. Zunger, Phys. Rev. B **85**, 085201 (2012).
[25] T. B. Boykin and G. Klimeck, Phys. Rev. B **71**, 115215 (2005).
[26] T. B. Boykin, N. Kharche, G. Klimeck, and M. Korkusinski, J. Phys.: Condens. Matter **19**, 036203 (2007).

[27] J. P. Perdew, K. Burke, and M. Ernzerhof, Phys. Rev. Lett. **77**, 3865 (1996).
[28] A. B. Kuzmenko, Rev. Sci. Instrum. **76**, 083108 (2005).
[29] B. Singh, A. Sharma, H. Lin, M. Z. Hasan, R. Prasad, and A. Bansil, Phys. Rev. B **86**, 115208 (2012).
[30] S. A. Mikhailov, Phys. Rev. B **83**, 155303 (2011).
[31] Y. Xiang, Q. Li, Y. Li, W. Xie, H. Yang, Z. Wang, Y. Yao, and H.-H. Wen, Nat. Commun. **12**, 6727 (2021).
[32] Y. Maeno, H. Hashimoto, K. Yoshida, S. Nishizaki, T. Fujita, J. G. Bednorz, and F. Lichtenberg, Nature (London) **372**, 532 (1994).
[33] E. Martino, I. Crassee, G. Eguchi, D. Santos-Cottin, R. D. Zhong, G. D. Gu, H. Berger, Z. Rukelj, M. Orlita, C. C. Homes, and A. Akrap, Phys. Rev. Lett. **122**, 217402 (2019).
[34] D. Santos-Cottin, M. Casula, L. de' Medici, F. Le Mardelé, J. Wyzula, M. Orlita, Y. Klein, A. Gauzzi, A. Akrap, and R. P. S. M. Lobo, Phys. Rev. B **104**, L201115 (2021).
[35] K. F. Mak, J. Shan, and T. F. Heinz, Phys. Rev. Lett. **106**, 046401 (2011).
[36] J. Ebad-Allah, J. F. Afonso, M. Krottenmüller, J. Hu, Y. L. Zhu, Z. Q. Mao, J. Kuneš, and C. A. Kuntscher, Phys. Rev. B **99**, 125154 (2019).
[37] D. Santos-Cottin, E. Martino, F. Le Mardelé, C. Witteveen, F. O. von Rohr, C. C. Homes, Z. Rukelj, and A. Akrap, Phys. Rev. Mater. **4**, 021201(R) (2020).
[38] F. Le Mardelé, D. Santos-Cottin, E. Martino, K. Semeniuk, S. B. David, F. Orbanić, M. Novak, Z. Rukelj, C. C. Homes, and A. Akrap, Phys. Rev. B **102**, 045201 (2020).
[39] S. Souma, M. Komatsu, M. Nomura, T. Sato, A. Takayama, T. Takahashi, K. Eto, K. Segawa, and Y. Ando, Phys. Rev. Lett. **109**, 186804 (2012).
[40] S.-Y. Xu, Y. Xia, L. A. Wray, S. Jia, F. Meier, J. H. Dil, J. Osterwalder, B. Slomski, A. Bansil, H. Lin, R. J. Cava, and M. Z. Hasan, Science **332**, 560 (2011).
[41] D. Santos-Cottin, J. Wyzula, F. Le Mardelé, I. Crassee, E. Martino, J. Novák, G. Eguchi, Z. Rukelj, M. Novak, M. Orlita, and A. Akrap, Phys. Rev. B **105**, L081114 (2022).
[42] M. Orlita, D. M. Basko, M. S. Zholudev, F. Teppe, W. Knap, V. I. Gavrilenko, N. N. Mikhailov, S. A. Dvoretskii, P. Neugebauer, C. Faugeras, A.-L. Barra, G. Martinez, and M. Potemski, Nat. Phys. **10**, 233 (2014).
[43] Z. Rukelj, C. C. Homes, M. Orlita, and A. Akrap, Phys. Rev. B **102**, 125201 (2020).
[44] J. Lim, K. J. A. Ooi, C. Zhang, L. K. Ang, and Y. S. Ang, Chin. Phys. B **29**, 077802 (2020).
[45] O. V. Kotov and Y. E. Lozovik, Phys. Rev. B **93**, 235417 (2016).
[46] Y. Shao, Z. Sun, Y. Wang, C. Xu, R. Sankar, A. J. Breindel, C. Cao, M. M. Fogler, A. J. Millis, F. Chou, Z. Li, T. Timusk, M. B. Maple, and D. N. Basov, Proc. Natl. Acad. Sci. USA **116**, 1168 (2019).
[47] C. Niu, Y. Dai, Y. Zhu, J. Lu, Y. Ma, and B. Huang, Appl. Phys. Lett. **101**, 182101 (2012).